The design of bacterial flagella: part 1—flagellar design in model organisms

David Thomas

For over two decades, the bacterial flagellum has been used as an example of design by the biblical creation and Intelligent Design communities after it was popularized by Michael Behe in *Darwin's Black Box*. Scientific knowledge of bacterial flagella and their associated systems has proliferated in recent years. This prolific knowledge is mainly due to recent advances in cryo-electron microscopy which have allowed us to visualize protein complexes at, or near, atomic resolution using an electron microscope. However, most of these discoveries have not been discussed in the creationist or Intelligent Design literature. This review will bring the reader up to date on these discoveries and will cover not just flagellar motors, but also their many associated control systems. Part 1 will look at the design of the flagella of the model organisms *Escherichia coli* and *Salmonella enterica*. Specifically, part 1 will focus on the function, atomic architecture, and design features of each of their parts. These parts come together to form a truly spectacular molecular machine.

> "When Antony van Leeuwenhoek looked through a single-lens microscope in 1676 and observed man's first recorded glimpse of bacteria, it was their motion that most delighted him: 'I must say, for my part, that no more pleasant sight has ever yet come before my eye than these many thousands of living creatures, seen all alive in a little drop of water, moving among one another, each several creature having its own proper motion.'"[1]

Bacterial movement has fascinated researchers since their discovery by the biblical creationist and father of microbiology Antonie van Leeuwenhoek.[2] At the scale of bacteria, water is like ultra-thick honey, since viscous forces dominate over inertial forces (represented with a low Reynolds number[3]). When a bacterium stops powered motion, it comes to a complete stop in less than a 10^{th} of the diameter of a hydrogen atom.[3] Despite this, bacteria swim through water incredibly quickly with one species reaching over 200 body lengths per second.[4] This is equivalent to a human swimming at 1,224 km/hr.

In the early 1970s, it was discovered that bacteria swim using nano-scale rotary motors that rotate long filaments that function as propellers.[5] The bacterial flagellar motor was popularized as an example of irreducible complexity by Michael Behe in his 1996 book *Darwin's Black Box* and has since become an icon of the Intelligent Design (ID) Movement. Scientific knowledge of bacterial flagella has proliferated in the last decade, due, in part, to cryo-electron microscopy (Cryo-EM). This technology has allowed researchers to image large protein complexes at, or near, atomic resolution using an electron microscope. The main advantages of Cryo-EM over X-ray crystallography is that Cryo-EM does not require the proteins to be crystallized and can capture large protein complexes *in situ*.[6]

Most of these recent discoveries have not been discussed in the creationist or ID literature. This review will bring the reader up to date on these discoveries and will cover not just flagellar motors, but also their many associated control systems.

This is a seven-part review (see table 1).

General information on bacterial flagella

- Bacterial flagella are typically divided into three main sections: a rotary motor, a helical propeller, and a universal joint which connects the motor to the propeller (figure 1).
- The motors are powered by the electrochemical potential (chemiosmotic/pH gradient) across the cell's cytoplasmic membrane and can be almost 100% efficient, depending on the conditions.[7]
- The fastest flagellar motor has been recorded at 102,000 rpm, which is ~8.5 times faster than a Formula One racing car engine.[8]
- Flagellar motors can change gears to change rotation direction, power output, fuel type, motor speed, and/or sensitivity to signals from the cell's navigation system (see parts 3 and 4).
- *E. coli's* bacterial flagellum is made of at least 27 proteins, each present in a few to tens of thousands of copies (table 2). In *E. coli*, over 12 other flagellar-associated proteins are required for flagellum assembly and regulation but are not part of the flagellum itself (table 2).
- Bacteria, archaea, and eukarya all include species with flagella, but their flagella each have radically different designs (figure 2).
- Bacterial flagella are just one of multiple different machines that bacteria use to move, most of which appear to involve a rotary motor.[9]

Table 1. Content of each part of this review

Part	What is covered
1	Design of the flagella in the model organisms *Escherichia coli* and *Salmonella enterica* (from now on, *E. coli* and *Salmonella*, respectively)
2	Diversity of flagellar designs across bacterial species, including the number and arrangement of flagella, the function of flagella, and the structure of flagella (of both core and additional parts)
3	Motility behaviour of bacteria and how flagellar motors change gears
4	Navigation systems that control flagellar motors, including chemotaxis systems
5	Gene regulation in flagellar-chemotaxis systems and how this controls construction of flagella and chemotaxis systems
6	Step-by-step mechanisms of how flagella and chemotaxis systems are constructed, including control mechanisms beyond gene regulation
7	Theoretical origin and evolution of flagellar-chemotaxis systems and an argument in favour of the creation/design explanation

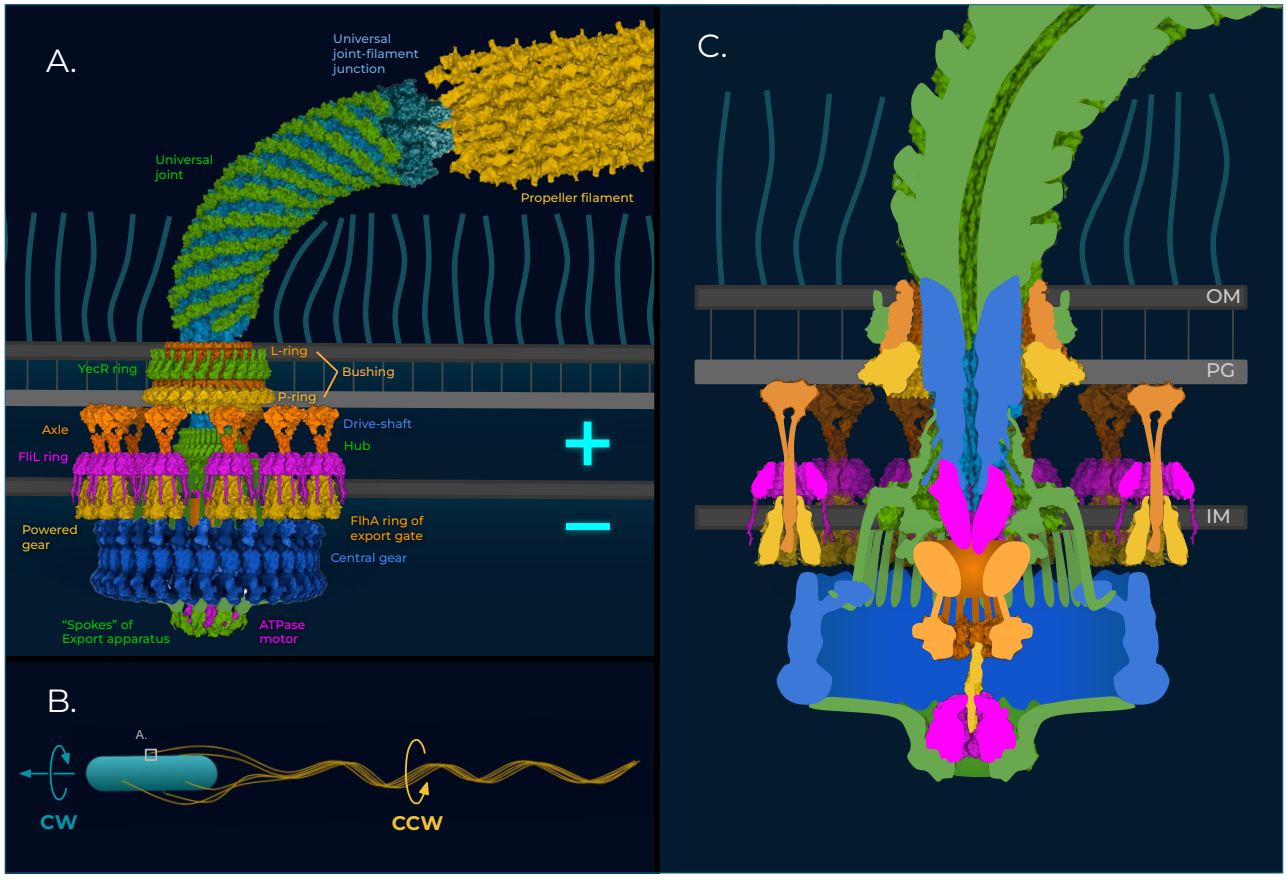

Figure 1. Bacterial flagellum of *E. coli*. (A) Representative illustration of *E. coli's* flagellar motor, which is near identical to *Salmonella's* flagellar motor. Illustration includes protein structures from *E. coli*, *Salmonella* and other species as well as Alphafold predictions[48,49] when the structure in *E. coli* has not yet been solved experimentally. The + and - symbols indicate the relative charge difference across the inner membrane of the cell. Labels are colour-coordinated to label the component closest to each label of the same colour (apart from the universal joint which is coloured green and blue but has a green label). (B) Illustration of a swimming *E. coli* cell showing the coordinated rotation of the propeller filaments. The blue arrows indicate the movement of the cell body and the yellow arrow indicates the rotation of the flagellar filaments. As well as propelling the cell forward, the CCW rotation of the filaments causes the cell to rotate CW. The square labelled 'A'. indicates the location of the close up shown in A. (C) Illustrative cross-section of *E. coli's* flagellar motor, coloured the same as in A (apart from the universal joint which is coloured green). The export apparatus located inside the motor can clearly be seen in this cross-section (see figure 9). OM: Outer membrane; PG: Peptidoglycan layer (cell wall); IM: Inner membrane. Unless stated otherwise, protein structures in all figures are sourced from the RCSB protein data bank[50] or the Alphafold protein structure database.[48,49] Protein graphics are made in part using Mol*.[51] The illustrations sometimes contain only parts of the cited PDB structures. The illustration of the central gear used in figures 1a, 2c, 3a, 6 and 7b is after Carroll *et al.*,[52] used with permission. The illustration of the universal joint-filament junction used in figures 1a, 2c and 21b is after Green *et al.*,[38] used with permission.

Table 2. Parts list for *Salmonella* and *E. coli* flagellar motors and their associated systems[10]

Common name(s) of part (alternative name)	Number of units*(Protein name$_{\text{number present}}$)	Function
Stator/torque-generating unit (powered gear and axle)	11*(MotA$_5$, MotB$_2$)	Converts electrical energy into kinetic energy (generate torque)
C-ring/switch complex (central gear)	33/34*(FliG, FliM, FliN$_3$)	Changes motor rotation direction. Transmit the torque of the powered gears to the central axis of the motor
FliL ring	11*(FliL$_{10}$)	Stabilizes the motor under high torque
Export gate	FliP$_5$, FliQ$_4$, FliR, FlhB, FlhA$_9$	Sorts and exports subunits to their assembly sites higher up in the flagellum
ATPase motor	FliJ, FliI$_6$	Unfolds and transports subunits to the export gate
Spokes	FliH$_{\text{unknown}}$	Hold the ATPase motor in place and stabilize the central gear
MS-ring (hub)	FliF$_{33/34}$	Connects the central gear, driveshaft, and export gate
Proximal rod (proximal driveshaft)	FliE$_6$, FlgB$_5$, FlgC$_6$	Transmits torque from the hub to the universal joint
Distal rod (distal driveshaft)	FlgF$_5$, FlgG$_{24}$	Transmits torque from the hub to the universal joint
P-ring (bushing)	FlgI$_{26}$	Stabilizes the rotation of the driveshaft
L-ring (bushing)	FlgH$_{26}$	Stabilizes the rotation of the driveshaft
YecR ring	YecR$_{26}$	May regulate the attachment between the outer membrane and the L-ring
Hook (universal joint)	FlgE$_{\sim 120}$	Changes the axis of rotation of the flagellum
Hook-filament junction (universal joint-filament junction)	FlgL$_{11}$, FlgK$_{11}$	Connects the universal joint to the filament
Filament (propeller)	FliC$_{>10,000}$, FljB$_{>10,000}$ (FljB only in *Salmonella*)	Exerts force on the surrounding fluid or substrate to move the cell
Filament cap	FliD$_5$	Assembles the filament
Flagellar proteins which are not part of the flagellum itself		
Master regulator	FlhD$_4$, FlhC$_2$	Activates Class ii flagella genes
FlgI chaperone	FlgA$_{\text{unknown}}$	Helps assemble the P-ring
Hook scaffold protein	FlgD$_5$	Assembles the hook
Hook length control	FliK$_{\text{many}}$	Controls hook length
FliO	FliO$_{\text{unknown}}$	Helps assemble the export gate
FlhE	FlhE$_{\text{unknown}}$	Unknown
Anti-sigma28 factor	FlgM	Inhibits Sigma28 (FliA)
FlgK/FlgL chaperone	FlgN	Binds to FlgK and FlgL
YdiV inhibitor	FliZ	Indirectly activates Class ii flagellar genes
Sigma28	FliA	Activates Class ii flagellar genes
FliD chaperone / anti-FlhDC factor	FliT	Binds to FliD and FlhC
Flagellin chaperone	FliS	Binds to Flagellin
FlgJ	FlgJ	N-acetylglucosaminidase
Chemotaxis proteins	Tar, Tap, CheR, CheB, CheY, CheZ, CheA, CheW	Form the chemotaxis system

Design of the parts

The similarities between flagellar motors and human-designed motors are simply astounding. Flagellar motors have many parts which perform similar functions to parts in human-designed motors, including gears, rotors, axles, driveshafts, bushings, ball-bearing–like bearings, brakes, clutches, structural scaffolds, hinges, universal joints, other joint types, adapter rings, sockets, switches, stators, capacitors, channels for fuel to flow through, mechanical sensors and components which respond to signals from the navigation system and other control systems.

The most studied bacterial flagella are those of the model organisms *E. coli* and *Salmonella*, which will be discussed below. Their differences will be pointed out when needed.

Gears

The gearbox of the motor is a 'two-cogwheel gear system'[11] (figure 3b) with a large central gear, surrounded by, and driven by, one or more smaller powered gears (figure 3a). The powered gears are powered by the electric voltage and chemical potential (difference in H^+ concentration) across the inner lipid membrane of the cell. This membrane functions as a capacitor by storing this electric voltage (and chemical potential), which is generated by other machines in the cell.

Each powered gear is made of five copies of a protein called MotA. These form a bell-shaped ring which rotates around an axle made of two copies of MotB (figures 4–5). The MotAB assembly is often called a stator or a torque-generating unit. The shape on one side of MotA matches the shape of the other side, like interlocking 3D puzzle pieces, allowing adjacent MotA subunits to tightly interlock. They interlock at a specific angle such that five of them form a ring. A band around the outer surface of the powered gear is hydrophobic, which keeps it positioned at the correct height in the lipid membrane (figure 4c).

MotB has three sections: the lower section functions as the axle inside the powered gear, the upper section functions as an anchor which attaches to the peptidoglycan cell wall, and the middle section functions as a tether between the axle and the anchor.[12] The axle is made of two alpha helices (one from each subunit) which twist around one another to form a coiled-coil structure which is the right diameter to fit inside the central hole of the powered gear.

The binding of protons to aspartate residues on the axle induces conformational changes which produce thrust. Based on the current evidence, protons flow through a stator complex through two channels between the axle and the powered gear. The movement of protons through these channels causes two aspartate residues on the outside of the axle to switch back and forth in a series of power strokes that each rotate the powered gear clockwise (when viewed from outside the cell) ~36°.[13] Based on detailed structural analysis, stators appear to use a sophisticated ratchet mechanism to prevent counterclockwise rotation.[14] Each power stroke is induced by the binding of one proton with each powered gear using 20 protons per rotation.[15] Each rotation step closes one channel and opens the other, resulting in a sequential operation. Thus, the 'stator' is itself a tiny rotary motor which powers the rotation of the larger components of the flagellum. This has been one of the most surprising discoveries in this field in recent years, because it was previously believed that the hub (MS-ring) and central gear (C-ring) formed the rotor, while the MotAB complex formed the stator. We now know that MotA forms the rotor and MotB forms the stator.

The tether section of MotB includes a region just above the axle called the 'plug region'. This region can plug the two proton channels through the powered gear, effectively turning it off (see part 3).

At the base of the powered gear, the five MotA subunits form five gear 'teeth'. Each tooth has specific amino acids at specific positions to form electrostatic interactions with specific amino acids at specific positions on the gear teeth of the central gear (figure 3c). The rotation of the powered gears drives the rotation of the central gear through these electrostatic interactions, analogous to man-made, contactless, magnetic gears.[16] It is not yet clear if the teeth of the gears are positioned in an interlocking orientation (tooth-to-gap) or if they line up tooth-to-tooth.[17]

If our current understanding is correct, the powered gears must rotate at 122,400 rpm in *E. coli* to drive the central gear at the measured speed of 18,000 rpm.[18] How these components can rotate so rapidly without forfeiting the integrity of the membrane remains to be solved.[19]

The central gear, commonly called the 'C-ring', is made of three stacked sections (figures 6–7; figures 1–26 are available here). The top section is made of FliG, which has three domains: the N-terminal domain connects to the hub; the middle domain connects to the middle section of the central gear; and the C-terminal domain forms the gear teeth (figure 7c). The middle section is made of FliM and changes confirmation to change motor rotation direction (see part 3). The lower section is made of FliN and the C-terminal of FliM and forms a coiled-coil structure (figure 7b–c).

The gear box of flagellar motors cannot function properly under high torque without a third important component of the gearbox—the FliL ring (figure 8).[20] In 2022, it was discovered that FliL forms a ring around the powered gears in *Helicobacter pylori* and *Borrelia burgdorferi* to stabilize them under high torque.[21,22]

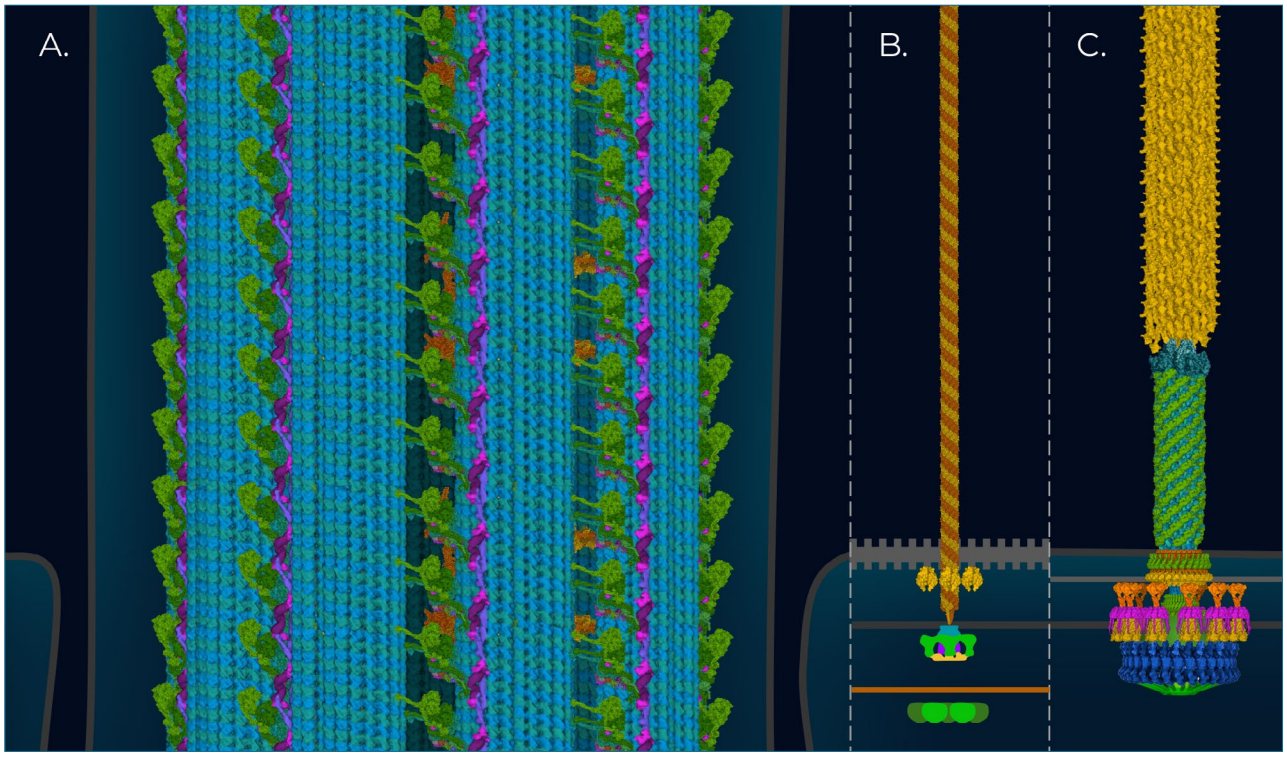

Figure 2. Comparison of flagella in eukarya (A), archaea (B), and bacteria (C). The universal joint of the bacterial flagellum is shown in a straight orientation for illustrative purposes and does not represent the wild-type structure of the universal joint. The archaeal flagellum is powered by ATP and has a propeller filament (PDB ID: 5TFY[53]) that is assembled from its base like a pilus, in contrast to bacterial flagellar filaments which are assembled from the tip (PDB ID: 4ZBH[54] is shown at archaellum base). The eukaryotic flagellum is by far the most complex, being made of over 400 different proteins that form an assembly of microtubules (shown in blue, PDB ID: 7RRO[55]), dynein (shown in green, PDB ID: 7K58[56]) and other components (shown in other colours, PDB ID: 7JTK[57]). Unlike archaeal and bacterial flagella, eukaryotic flagella do not rotate but sway side to side. See the caption of figure 1 for image credit for C.

Export apparatus

Sitting inside the central gear and hub is a molecular machine called the export apparatus. The export apparatus has three components: an export gate, an ATPase motor, and a ring of spokes (figure 9). Since this apparatus is involved in the construction of flagella, its design will be discussed in part 6.

Hub

The hub (figures 10–11), commonly called the MS-ring, has a remarkably complex structure, especially considering that it is made of a single type of protein called FliF. The hub is a ring complex made of 33 copies of FliF and sits in the inner membrane.[23] The hub forms the connection between the driveshaft, central gear, and export gate. In mechanical terms, the central gear and hub can together be called the 'transmission'.

FliF likely has 6 domains, though its complete structure has not yet been solved. At the top of the hub is a beta-collar called the 'socket', which houses the base of the driveshaft. The upper section of the socket has a smaller diameter than the lower section, which prevents the driveshaft from slipping out (figure 10c).[24] Around the base of the socket is an outer ring formed by domain RBM3. The C-terminal of FliF extends from the outer ring and hooks around the N-terminal domain of FliG to connect the hub and central gear (figure 11d).[25]

The socket and outer ring have 33-fold rotational symmetry to match the rotational symmetry of the central gear.[23] The central gear and hub can also have 34-fold rotational symmetry[26,25] (see part 4). The hub has an inner ring of 21-fold rotational symmetry, which has structural plasticity to mold to the irregular helical shape of the export gate which it holds in place.[27] Consequently, the inner ring functions as a symmetry adapter between the rotational symmetry of the outer ring and the helical symmetry of the export gate. Another component of the hub forms a rotational symmetry adapter ring, linking the outer ring, with 33-fold rotational symmetry, and the inner ring, with 21-fold rotational symmetry. Remarkably, the inner ring and adapter ring are both made of the same domain of FliF, RBM2, but

are derived from different subunits (figure 11a–c): Of the 33 RBM2 domains present in the structure, 21 form the inner ring, nine form the adapter ring, and the locations of the remaining three are unknown.[23] (When the hub contains 34 RBM2 domains, 22 form the inner ring while 10 form the adapter ring,[23] or, according to another study, 23 form the inner ring while 11 form the adapter ring.[25]) The subunits around the hub therefore fold into different conformations to form these different structures (figure 11b–c). For this design to work, the RBM2 domains must have the appropriate binding sites and shape to form both the inner ring and the adapter ring. The hub's design, with multiple different rings of different symmetries all forming from a single type of protein, explains a long-unresolved mystery in the field as to why the hub and central gear had observed differences in their rotational symmetry.

The RBM1 domains and N-terminals of FliF likely extend from the base of the adapter and inner rings to form a ring around the FlhA ring of the export gate (figures 1c, 9, 11d).[23]

Driveshaft

Torque is transmitted from the hub inside the cell to the universal joint outside the cell via a driveshaft which passes through a bushing (a type of bearing) (figure 12). At the start of 2021, the atomic structure of the driveshaft and bushing was not known. Then, in April, May, and July 2021, three separate teams of scientists published the atomic structures of the driveshaft and bushings of *Salmonella*.[24,27,28] Below are their findings.

The design of the driveshaft, often called the 'rod', is anything but simple (figures 13–14). The proximal driveshaft has 17 subunits (6 FliE, 5 FlgB, and 6 FlgC), while the distal driveshaft has 29 subunits (5 FlgF and 24 FlgG). The proximal driveshaft slots on top of the export gate inside the hub socket and strongly attaches to both. The distal driveshaft is thicker and sits inside the bushing. The driveshaft subunits form 11 rows, called 'protofilaments', which twist in a left-handed helix.

The driveshaft must be strong, straight, and highly rigid to efficiently transfer torque from the hub to the universal joint. It also experiences a lot of mechanical stress and so must be highly reinforced to prevent it from breaking apart. The inner layer of the driveshaft and the outer layer of the distal driveshaft are both highly reinforced in specific directions to provide strength and rigidity. Each subunit in the driveshaft is precisely shaped to tightly interlock and forms extensive connections with adjacent subunits.[24] The Dc domains of FlgG in the upper distal driveshaft extend downwards and connect to the subunits in the lower distal driveshaft (FlgG and FlgF) and the proximal driveshaft (FlgC). This tightly connects the distal and proximal driveshafts and tightly connects the inner and outer layers of the structure. The inner layer is made of alpha helices which slot together like tiles on a roof.

The proteins that form the distal driveshaft are shaped in such a way that when they interlock, they leave a small hole between them in the outer layer. In the lower portion of the distal driveshaft, these holes are filled in with a section of the FlgG subunits called the 'FlgG specific sequence' (labelled GSS in figure 14b), which interacts with the three surrounding subunits (figure 13a). This reinforces the lower distal driveshaft. However, in the upper portion of the distal driveshaft these holes are not filled in because the universal joint subunits do not have the GSS region (figure 14b). This makes the upper portion of the distal driveshaft slightly more flexible. This likely makes for a smoother transition between the rigid lower distal driveshaft and the flexible universal joint, which would allow for more efficient torque transmission between these components.

The driveshaft is at risk of breaking apart from the hub and export gate due to the mechanical strain experienced under high torque. To prevent this, it is strongly attached to the hub and export gate in multiple different locations (figure 15a). The proximal driveshaft slots into the top of the export gate (figure 15d). Alpha helices from both components grip onto grooves on the adjacent component.

The proximal driveshaft also attaches to the inner surface of the hub socket. FliE alpha helices bind to the lower inner surface of the hub socket, while FlgB binds to the upper inner surface of the hub socket (figure 15d). These subunits have flexible adapter regions which allow them to function as adapters between the hub with rotational symmetry and the driveshaft with helical symmetry.

The hub also connects to the proximal driveshaft. Peptide loops with regions called 'L1' and 'L2' extend out of the top of the hub socket from each of the FliF subunits. Five of the L1 regions bind into grooves in the proximal driveshaft while five of the L2 regions bind into open pockets in the proximal driveshaft (figure 15b–c). Flexibility in the FliF loops allows them to bind at different heights around the helical driveshaft, allowing them to also function as symmetry adapters between the hub and driveshaft.[27]

Bushing

The distal driveshaft rotates inside a cylindrical structure which functions as a bushing (figures 12, 16–18). The bushing is made of two rings called the 'L-' and 'P-rings'. The P-ring sits in the cell wall, surrounds the lower distal driveshaft and is made of 26 interlocking FlgI subunits. The L-ring sits in the outer membrane, surrounds the upper end of the distal driveshaft and is made of 26 interlocking FlgH subunits. The inner surface of the bushing and the

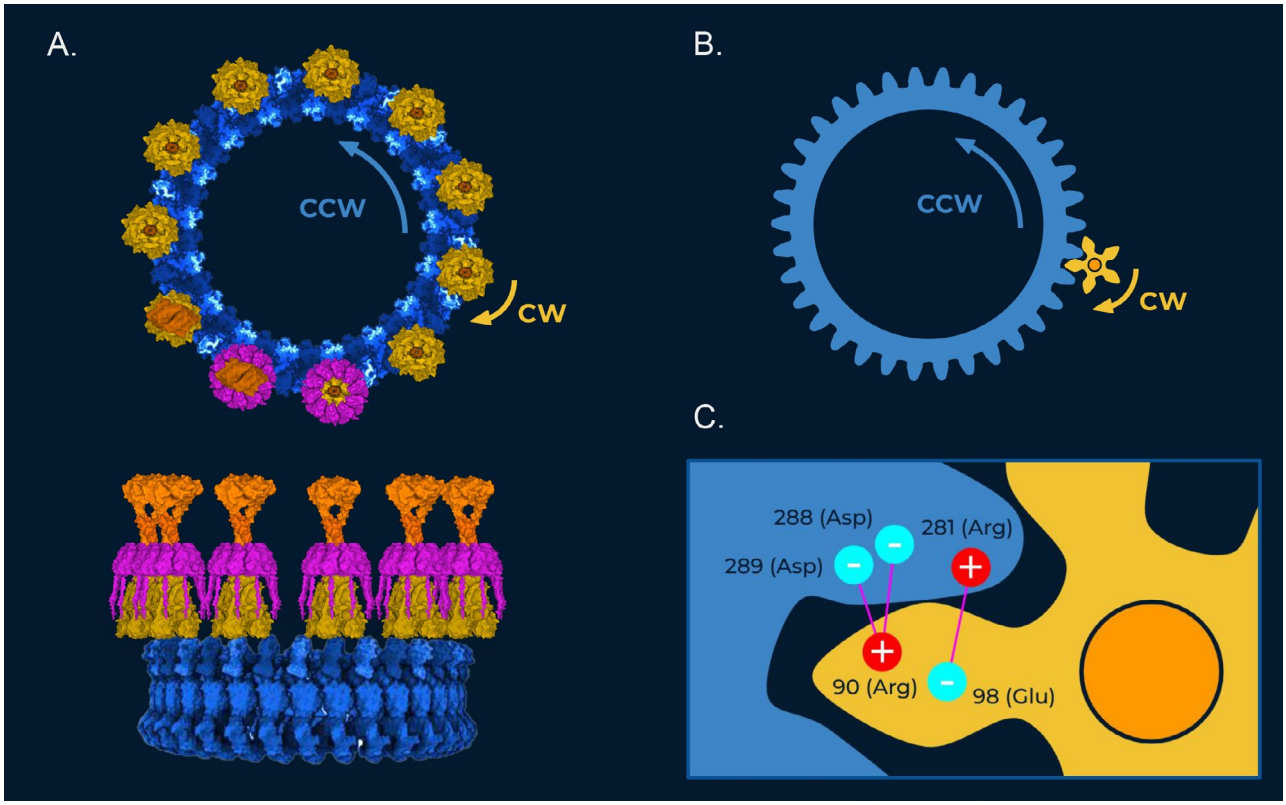

Figure 3. Representative illustration of the gearbox of the flagellar motor of *E. coli* and *Salmonella* in forward gear at full power. (A) Molecular surface representation of the gearbox viewed from the top (top) and side (bottom). In the top view, one MotA powered gear is shown with the cell-wall binding domain of MotB (shown in orange), one with the FliL ring (shown in purple) and one with both. The rest of the power gears are shown only with the axle domain of MotB (shown in orange). See the caption of figure 1 for image credit. (B) Diagram of a two-cogwheel system with a gear ratio of 34:5. (C) Residues involved in electrostatic interactions between the central gear and powered gears. Residue numbers correspond to sequences in *E. coli.* It is possible that the gear teeth are not in an interlocking orientation but are oriented with the gear teeth of the power gear positioned directly above the gear teeth of the central gear.

outer surface of the distal driveshaft are each very smooth, "indicating that these two structures are optimally designed for free rotation of the [driveshaft] inside the LP ring without much friction."[28] This smoothness is remarkable when compared to the typically bumpy surface of proteins.

The P-ring is made of three subrings corresponding to the three domains of FlgI (figure 17). The P-ring is highly reinforced with tight connections between the three subrings and between adjacent subunits. The inner subring of the P-ring (made of domain D1) forms a water-tight seal around the distal driveshaft. This seal contacts the distal driveshaft at a knife-edge to greatly minimize friction. To further minimize friction, this knife-edge seal is believed to form a ring of hydrogen bonds with the distal driveshaft which "allow[s] the P ring to act as a ball bearing to stabilize the central localization of the [driveshaft] in the P ring and enable rotation of the distal [driveshaft] without significant structural obstacles or energy consumption."[24] The symmetry mismatch between the driveshaft and P-ring (helical and rotational, respectively) further reduces friction, allowing the driveshaft to rotate more smoothly.[27]

The gap between the bushing and driveshaft must be small enough to stop fluids leaking out of the cell but large enough that the bushing does not grip the driveshaft too tightly. This is an insanely small margin for error. The gap between the knife-edge seal of the P-ring and the distal driveshaft is less than the diameter of a carbon atom (< 0.34 nm).[29] Thus, the diameter of the driveshaft and bushing are fine-tuned with atomic-scale accuracy. To get this level of accuracy, the subunits that make these parts must have a precise shape, width, and binding angle to form a helical tube or ring, respectively, with the right diameters.

The bottom section of the distal driveshaft is made of FlgF, instead of FlgG, and has a diameter that is slightly larger than the diameter of the hole through the bushing. This "precisely coordinates the position of the [driveshaft]"[24] within the bushing by reducing vertical sliding of the driveshaft.

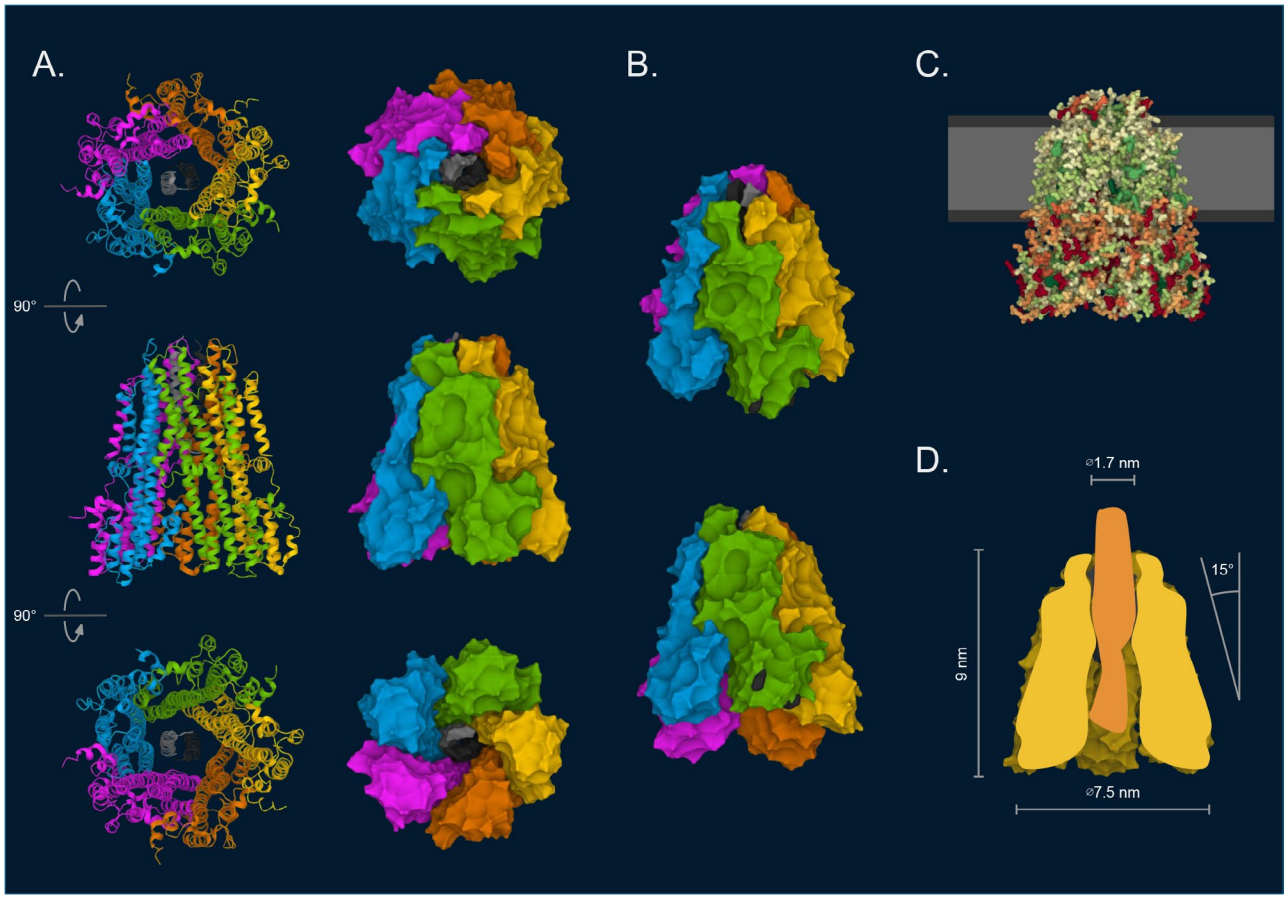

Figure 4. The MotA powered gear of *Bacillus subtilis* (PDB ID: 6YSL[13]), which is expected to be very similar to that in *E. coli* and *Salmonella*. (A) The ribbon diagram (left) and molecular surface representation (right) of the MotA powered gear. The MotB axle is shown in light and dark gray. (B) Isometric views of MotA powered gear. Residues that form electrostatic interactions with the central gear (90 and 98 in *B. subtilis*) have been coloured dark gray on the green MotA subunit. (C) Hydrophobicity of residues (red = hydrophilic; green = hydrophobic). The approximate positions of the hydrophilic and hydrophobic portions of the cytoplasmic membrane have been shown in dark gray and light gray, respectively. (D) Illustrative cross-section of MotA powered gear (yellow) and MotB axle (orange).

The outer perimeter of the P-ring is designed to tightly attach to the cell wall. This is necessary to fix the bushing in place. The L-ring must be strongly attached to the top of the P-ring to hold it in the correct position and alignment around the driveshaft. Thus, each subunit in the L-ring binds to four subunits in the P-ring.[24]

The L-ring has three layers. The inner two layers form a beautifully elegant double-layered beta sheet cylinder (figure 17b). The beta strands in the two layers are angled at 85° to one another to form a strong lattice structure with cross-links between the layers. Each subunit in the L-ring intricately interlocks with six adjacent subunits to form a very mechanically stable structure.[28]

For proper function, the L-ring must connect to the outer membrane. Around the top of the L-ring is a hydrophobic band made of two rings of alpha helices (figure 18a,c). The third layer is made by the N-terminal of FlgH. The tip of the N-terminal has a fatty acetyl group attached which inserts into a hydrophobic gap between the alpha helices in the lower ring of alpha helices. This forms a tighter connection between the L-ring and outer membrane. A membrane-bound, lipidated protein called 'YecR' binds around the outside of the L-ring and is believed to regulate the attachment between the outer membrane and the L-ring (figure 18).[27]

A band around the top of the inside of the L-ring is strongly negatively charged, which repels the negatively charged distal driveshaft. This is believed to stabilize the central position of the distal driveshaft as it rotates.[24] In contrast, the knife-edge seal of the P-ring is positively charged and is thus attracted to the negatively charged distal driveshaft, which may be important for the construction of the P-ring around the distal driveshaft (see part 6).

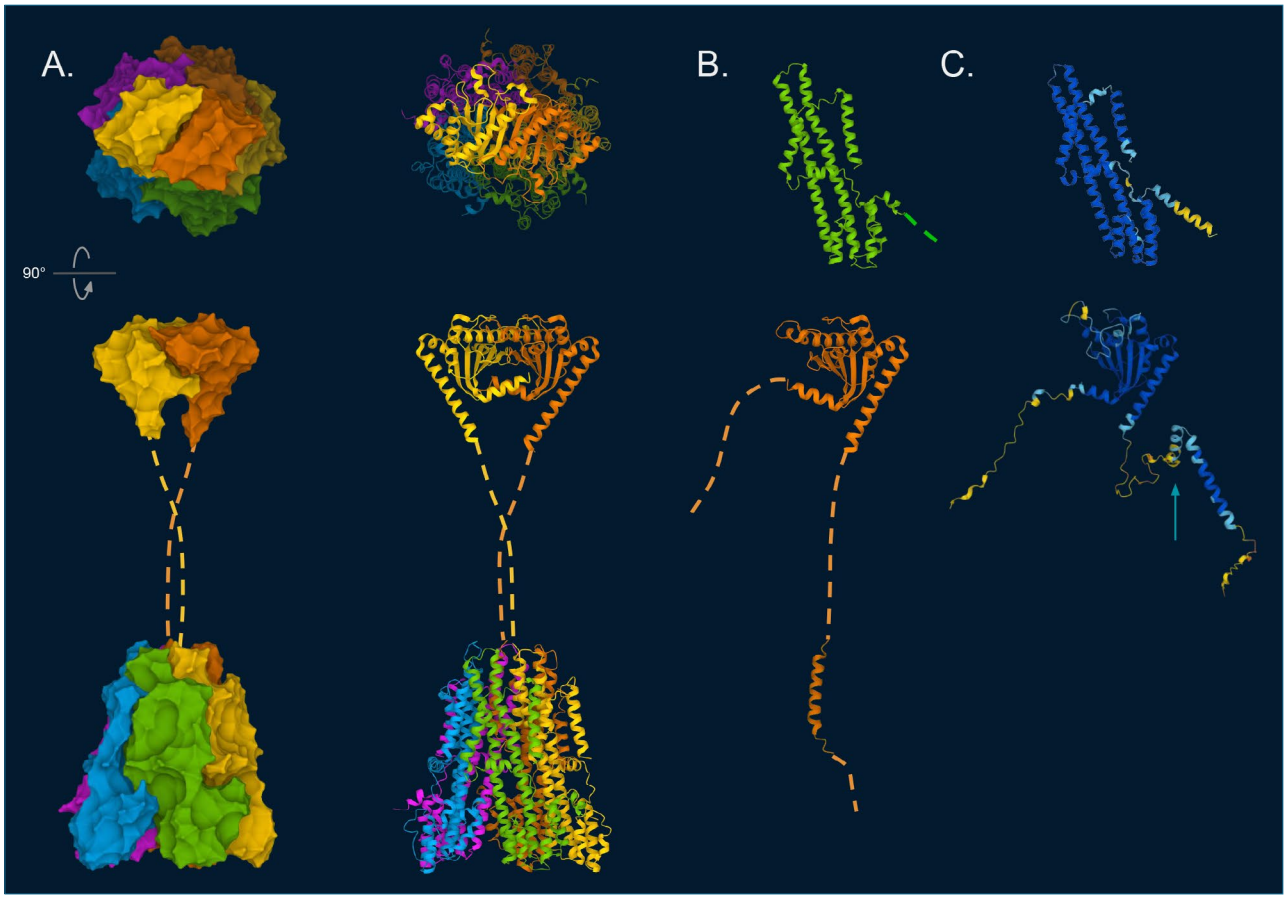

Figure 5. The MotAB complex of *Bacillus subtilis*. (A) The molecular surface representation (left) and ribbon diagram (right) of the MotAB complex. MotA subunits (PDB ID: 6YSL) shown in blue, green, yellow, orange and purple, respectively. MotB subunits (PDB IDs: 2ZVY[58] & 6YSL) shown in yellow and orange, respectively. (B) The solved structure of MotA (upper) and MotB (lower). The dashed lines indicate portions of the structures that have not been solved experimentally and are likely unstructured (apart from the plug region). (C) The Alphafold prediction of MotA (upper, P28611) and MotB (lower, P0AF07), showing portions of proteins not yet solved (dark blue = very high confidence in prediction accuracy, orange = very low confidence). The blue arrow points to the plug region of MotB.

Universal joint

Torque is smoothly transmitted from the driveshaft to the propeller filament using a sophisticated universal joint (figures 19–20). The sophistication of this joint surpasses what was expected even by ID advocates.[30] Unlike the driveshaft, which must be rigid, the universal joint must be longitudinally flexible and rotationally rigid (easy to bend but hard to twist), placing significant constraints on its design.

The universal joint, composed of approximately 120 FlgE subunits, forms a curved structure with three tubular layers, each possessing distinct mechanical properties.[31,32] The three layers are made of the four domains of FlgE (the middle layer is made of two domains, D1 and Dc). The domains are each quite rigid but have flexible hinges between them.[33] These hinges allow each side of the universal joint to smoothly expand and contract as it rotates. The smooth compression and extension is guided by dynamic changes in the interactions between adjacent subunits, allowing the structure to flex with minimal energy cost.[32,34]

When the motor is operating at full speed, the sides of the universal joint in *E. coli* expand and contract approximately 300 times per second.[35] Yet, even at such high speeds the universal joint can smoothly and efficiently transmit the torque from the motor to the propeller filament.

The inner layer has a very similar design to the inner layer of the driveshaft. The middle layer forms a mesh-like structure which is reinforced in three different helical directions.[32] This gives the universal joint its necessary rotational rigidity and strength, while still allowing longitudinal flexibility.[33] The outer layer forms a six-stranded helical structure that resembles a spring.[32] Each domain in the spiral tightly interacts with adjacent domains around the spiral for mechanical support.

Since the hook experiences high mechanical strain, it is intricately attached to the driveshaft to prevent breakage (figure 20c). Also, the Dc domains of the universal joint hook under the subunits in the distal driveshaft (they hook into the holes between the driveshaft subunits but do not have the GSS region to fill the holes and so do not provide rigidity).[24] This tight connection between the driveshaft and universal joint allows for efficient torque transmission between them.

The length of the universal joint is optimized to 55 ± 6 nm.[31] It is believed that if the universal joint were too long, it would buckle and cause the flagellar filament bundle behind the cell to be less stable, making the cell body wobble and swim less efficiently. Alternatively, if it were too short, it would be too stiff to function as a universal joint.[36]

The universal joint must possess sufficient flexibility to accommodate the large change in axis of rotation while also maintaining rigidity to prevent breakage under significant hydrodynamic stress. To solve this, when the hydrodynamic forces on the propeller filament increase, the universal joint automatically stiffens to reduce the bending angle.[37] This allows the universal joint to fine-tune its stiffness in response to solution thickness, necessary for efficient, high-speed swimming.

Universal joint–filament junction

The universal joint–filament junction connects the flexible universal joint to the more rigid propeller filament (figure 21).[31] It comprises two adapter rings made from FlgK and FlgL, respectively.[38] Its complete atomic structure is yet to be solved.

Propeller filament

The final component of the flagellum, not including the filament cap, which is used during construction and stays attached at the tip, is the filament (figures 22–25). The driveshaft, universal joint, universal joint–filament junction, and the filament are collectively referred to as the 'axial components' (figure 26a). This contrasts with the torque-generating units, central gear, hub, and bushing, which are referred to as the 'ring components' (figure 26b).

When rotated counterclockwise, the long screw-shaped filament propels the cell forward (figure 1b). In *E. coli*, each filament is made of tens of thousands of FliC subunits, is about 20 nm wide and 15 µm long.[39] *Salmonella* alternates as to whether its filaments are made of FliC or FljB every few generations in a process called 'flagellar phase variation' (see part 5).[40] The outer domain of FljB is more flexible than that of FliC and allows for closer to optimum motility under viscous conditions.[41] Collectively, flagellar filament proteins are referred to as 'flagellin'.

The core of the filament structure is a rigid, highly reinforced double-layered tube.[42] Like the driveshaft and universal joint, the filament is made of 11 twisted protofilaments.

To function as a propeller, the filament must form a rigid helix. It is no small engineering challenge to get a filament made of a single type of protein to form a supercoiled helical shape. It is believed that this is achieved by the protofilaments existing in two distinct conformations, with each protofilament able to flick between a contracted or expanded form.[34] If one side of the filament is contracted and the other is expanded, the filament is curved, and because the filament is also twisted, it forms a helix.

Three different types of interactions between the subunits are essential for this design to work: Firstly, 'permanent' interactions determine the geometrical constraints of the filament's architecture. Secondly, 'sliding' interactions allow subunits to slide past each other with minimal changes in interaction energy. Thirdly, 'switch' interactions stabilize the protofilament's two conformations.[34] Evidence indicates that the protofilaments are in an intricate balance between expanded and contracted forms and can rapidly flick between them.[39] Single point mutations can cause the protofilaments to be either all expanded or all contracted, which results in a non-motile mutant with straight filaments.[39] This places very tight constraints on the design of the filament.

The filament is not just a simple propeller: modifying how many protofilaments are contracted or expanded changes the helical pitch and diameter of the filament to form many different waveforms which are used during swimming and turning manoeuvres.[43] When a filament is rotated counterclockwise (looking from behind the cell), the torque exerted on the filament by the motor causes it to form a rigid left-handed helical shape, perfect for a propeller. However, when the filament is rotated clockwise, it forms a right-handed helix.

When all the filaments of a cell are rotated counter-clockwise, the filaments all come together in a coordinated bundle behind the cell, which propels the cell forward (figure 1b).[44] To form a smoothly rotating filament bundle without jamming, the filaments must rotate in phase with each other. The filaments use an elastohydrodynamic mechanism to do this.[45] The elastic properties of the universal joint and filament are crucial for this mechanism to work, without which the cells would be unable to swim straight.[45] When one or more filaments are rotated clockwise, they change their waveform, separate from the filament bundle and turn the cell in a new direction (see parts 3 and 4).[43]

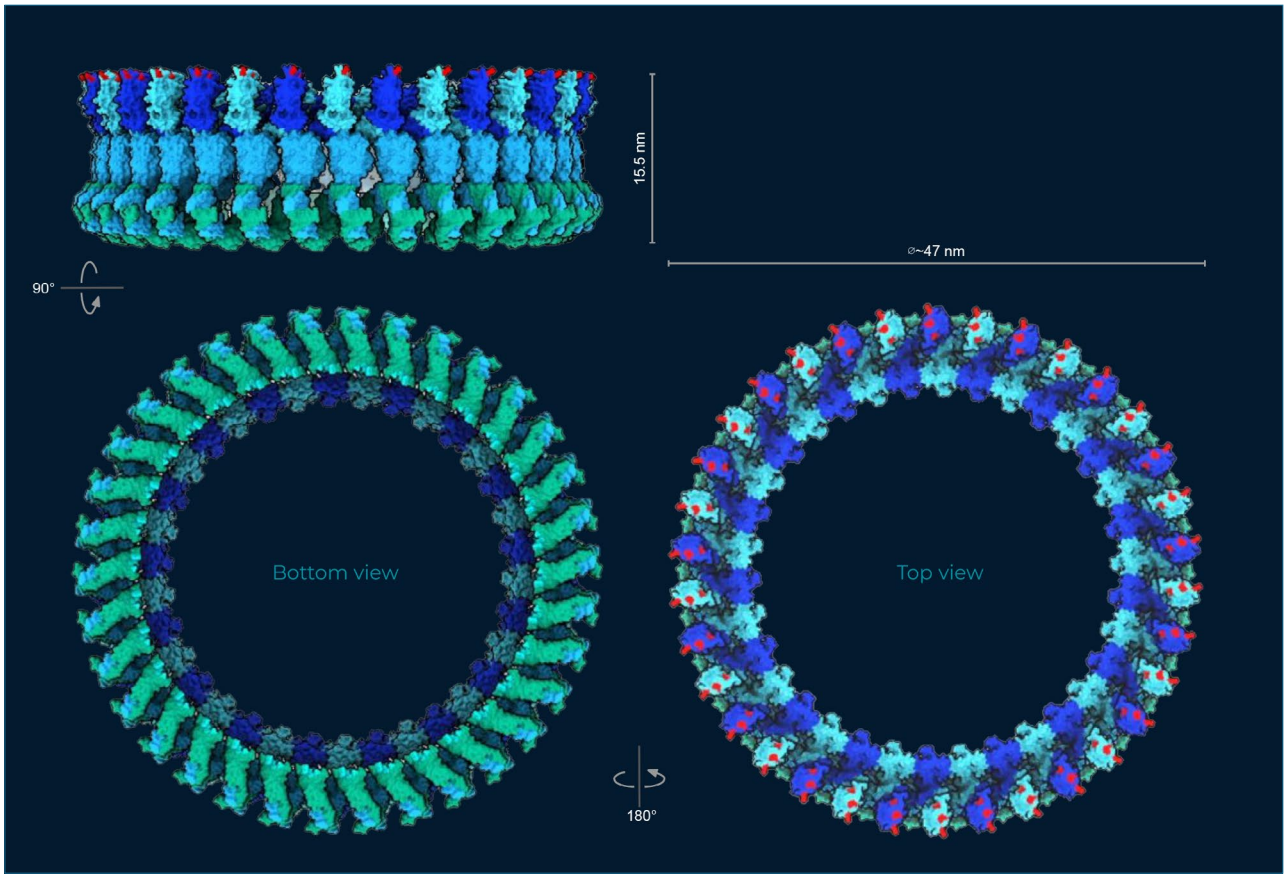

Figure 6. Orthographic projection of the predicted structure of the central gear (C-ring) of *Vibrio alginolyticus* which is believed to have a very similar structure to the central gear of *E. coli* and *Salmonella*. FliG is shown in dark blue and cyan, FliM is shown in light blue, and FliN is shown in green. FliG residues which form electrostatic interactions with MotA are shown in red. See the caption of figure 1 for image credit.

The design of the flagellar filaments has become even more remarkable with the discovery that the outer domains of FliC in some bacteria, including some *E. coli* strains, can form a beautifully complex sheath around the filament core with different symmetry to the core structure.[46] The outer domains can form tetramers (in the *E. coli* O127:H6, figure 22) or dimers (in the *E. coli* O157:H7, figure 23).[46]

Conclusion

Bacterial flagella are truly an engineering marvel; every minute detail of every part of these flagella is intricately and beautifully designed. Each part is not designed in isolation but is designed to work together with the other parts as a complete functioning whole. All of these parts, each with their own remarkable design features, come together to form a truly spectacular molecular machine.

Leeuwenhoek saw none of this, and yet I'm sure he would say, as he did in his day:

> "From all these observations, most plainly we discern the incomprehensible perfection, the exact order, and the inscrutable providential care with which the most wise Creator and Lord of the Universe has formed the bodies of these Animalcules … . And this … must surely convince all of the absurdity of those old opinions, that living creatures can be produced from corruption or putrefaction."[47]

Part 2 will explore the design of flagella from other species which are significantly more complex than those discussed here and contain many additional parts. As it turns out, the flagella of *E. coli* and *Salmonella* may be two of the simplest within bacteria.

Acknowledgments

I'd like to thank the following people who gave their time to read over the drafts of this paper and provide me with helpful feedback: Christopher Sernaqué, Intelligent Design advocate Waldean (Dean) Schulz, and Ben R. I'd like to especially thank Dr Andrew Fabich for our many discussions over Zoom to help me improve the paper. Any remaining mistakes are solely my own.

References

1. Berg, H.C., How bacteria swim, *Scientific American* ***233***:36–45, 1975. Howard Berg (1934–2021) did important work studying bacterial chemotaxis. He was also the first to propose, in 1973, that flagella rotate. This "overturned the long-held notion that rotation could not exist in living organisms". Blair, D. and Manson, M., Howard Berg (1934–2021), *Current Biology* **32:**R252–R254, 2022.
2. Nouri, A., The discovery of bacteria, *Scientia,* 2011; aaas.org. See also, Grigg, R., Antony van Leeuwenhoek: Discoverer of bacteria and refuter of spontaneous generation, *Creation* **41**(2):52–55, 2019; Antony van Leeuwenhoek | creation.com.
3. A classic paper: Purcell, E., Life at low Reynolds number, *American J. Physics* **45**:3–11, 1977.
4. Bente, K., Mohammadinejad, S., Charsooghi, M.A., Bachmann, F., Codutti, A., Lefèvre, C., Klumpp, S., and Faivre, D., High-speed motility originates from cooperatively pushing and pulling flagella bundles in bilophotrichous bacteria, *eLife* **9**:e47551, 2020.
5. Berg, H. and Anderson, R., Bacteria swim by rotating their flagellar filaments, *Nature* **245**:380–382, 1973.
6. Chua, E.Y.D., Mendez, J.H., Rapp, M., Ilca, S.L., Tan, Y.Z., Maruthi, K., Kuang, H., Zimanyi, C.M., Cheng, A., Eng, E.T., Noble, A.J., Potter, C.S., and Carragher, B., Better, faster, cheaper: recent advances in cryo-electron microscopy, *Annual Review of Biochem.* **91**:1–32, 2022.
7. Li, G. and Tang, J.X., Low flagellar motor torque and high swimming efficiency of Caulobacter crescentus swarmer cells, *Biophysical J.* **91**:2726–2734, 2006. See also, Brewer, P., Peltzer E., and Lage, K., Life at low Reynolds number re-visited: the efficiency of microbial propulsion, *Deep Sea Research Part I: Oceanographic Research Papers* **185**:103790, 2022. Much of the energy from the flagellum likely actually goes into breaking hydrogen bonds in the water around the cell. This is crucial for producing the viscous flow needed for the cell's highly efficient swimming.
8. Yamaguchi, T., Makino, F., Miyata, T., Minamino, T., Kato, T., and Namba, K., Structure of the molecular bushing of the bacterial flagellar motor, *Nature Commun.* **12**:4469, 2021. See also, Magariyama, Y., Sugiyama, S., Muramoto, K., Maekawa, Y., Kawagishi, I., Imae, Y., and Kudo, S., Very fast flagellar rotation, *Nature* **371**:752, 1994.
9. For an overview of other bacterial motility machines, see: Wadhwa, N. and Berg, H.C., Bacterial motility: machinery and mechanisms, *Nature Rev. Microbiol.* **20**:161–173, 2022.
10. Some of these proteins, such as FlhD and FlhC, serve functions beyond the flagella-chemotaxis system. For more details, see part 5.
11. Peil, A., Xin, L., Both, S., Shen, L., Ke, Y., Weiss, T., Zhan, P., and Liu, N., DNA assembly of modular components into a rotary nanodevice, *ACS Nano* **16**:5284–5291, 2022.
12. Zhu, S., Takao, M., Li, N., Sakuma, M., Nishino, Y., Homma, M., Kojima, S., and Imada, K., Conformational change in the periplasmic region of the flagellar stator coupled with the assembly around the rotor, PNAS **111**:13523–13528, 2014.
13. Deme, J.D., Johnson, D., Vickery, O., Muellbauer, A., Monkhouse, H., Griffiths, T., James, R.H., Berks, B.C., Coulton, J.W., Stansfeld, P.J., and Lea, S.M., Structures of the stator complex that drives rotation of the bacterial flagellum, *Nature Microbiol.* **5**:1553–1564, 2020.
14. Taylor. N., Hu, H. Popp. P., Santiveri, M., Roa-Eguiara, A., Yan, Y., Liu, Z., Wadhwa, N., Wang, Y., and Marc, E., Ion selectivity and rotor coupling of the Vibrio flagellar sodium-driven stator unit, *Research Square preprint.*
15. Wang, B., Yeu, G., Zhang, R., and Yuan, J., Direct measurement of the stall torque of the flagellar motor in *Escherichia coli* with magnetic tweezers, *Molecular and Cellular Biol.* **13**(4), 2022. The number of protons used per revolution of the central gear depends on the number of powered gears engaged with the central gear and the gear ratio between them, which differs over time and between species.
16. For a video of contactless magnetic gears in an interlocking orientation, see: Neo Dyne, MAGS—magnetically assisted gears, MAGS - magnetically assisted gears | youtube, 17 Oct 2018.
17. From a design perspective, either would work. Deme *et al.*, ref. 13 suggests that the central gear teeth ($FliG_C$) may be located between two neighbouring MotA subunits, because the residues which interact with FliG are located on opposite sides of the MotA subunit.
18. Gear ratio of 34:5. 34/5 × 18,000 = 122,400 rpm. For direct measurements of rotation speed and torque in *E. coli*, see Wang *et al.*, ref. 15.
The fastest recorded rotation speed of a flagellar motor is 102,000 rpm; in: *Vibrio alginolyticus* (Magariyama *et al*., ref. 8). The powered gears of *V. alginolyticus* may be spinning close to a million rpm.
19. Assuming that the system is designed will greatly accelerate finding the solution to this question and many others like it within the field. See the following video on Dr Paul Nelson's Intelligent Design–based principle of design triangulation, which is used by biologists frequently, even if they do not believe the systems are actually designed: Origins: Design Triangulation | YouTube.
20. Backman, I., How bacteria swim: researchers discover new mechanisms | Phys.org, 4 Apr 2022.
21. Tachiyama, S., Chan, K.L., Liu, X., Hathroubi, S., Li, W., Peterson, B., Khan, M.F., Ottemann, K.M., Liu, J. and Roujeinikova, A., The flagellar motor protein FliL forms a scaffold of circumferentially positioned rings required for stator activation, PNAS **199**(4):e2118401119, 2022.
22. Guo, S., Xu, H., Chang, Y., Motaleb, M.A., and Liu, J., FliL ring enhances the function of periplasmic flagella, PNAS **119**(11):e211724511, 2022.
23. Johnson, S., Fong, Y.H., Deme, J.C., Furlong, E.J., Kuhlen, L., and Lea, S.M., Symmetry mismatch in the MS-ring of the bacterial flagellar rotor explains structural coordination of secretion and rotation, *Nature Microbiol.* **5**:966–975, 2020.
24. Tan, J., Zhang, X., Wang, X., Xu, C., Chang, S., Wu, H., Wang, T., Liang, H., Gao, H., Zhou, Y., and Zhu, Y., Structural basis of assembly and torque transmission of the bacterial flagellar motor, *Cell* **184**:2665–2679, 2021.
25. Kawamoto, A., Miyata, T., Makino, F., Kinoshita, M., Minamino, T., Imada, K., Kato, T., and Namba, K., Native flagellar MS ring is formed by 34 subunits with 23-fold and 11-fold subsymmetries, *Nature Commun.* **12**:4223, 2021.
26. Carroll, B.L., Nishikino, T., Guo, W., Zhu, S., Kojima, S., Homma, M., and Liu, J., The flagellar motor of *Vibrio alginolyticus* undergoes major structural remodeling during rotational switching, *eLife* **9**:e61446, 2020.
27. Johnson, S., Furlong, E.J., Deme, J.C., Nord, A.L., Caesar, J., Chevance, F., Berry, R.M., Hughes, K.T., and Lea, S.M., Molecular structure of the intact bacterial flagellar basal body, *Nature Microbiol.* **6**:712–721, 2021.
28. Yamaguchi, T., Makuno, F., Miyata. T., Minamino, T., Kato. T., and Namba, K., Structure of the molecular bushing of the bacterial flagellar motor, *Nature Commun.* **12**:4469, 2021.
29. Using a van der Waals radius for a carbon atom of 0.17 nm. For information on the flagellar driveshaft–bushing gap width, see: Tan *et al.*, ref. 24.
30. An icon revisited: flagellar hook shows further aspects of design | Evolution news, Oct 2019.
31. Samatey, F.A., Matsunami, H., Imada, K., Nagashima, S., Shaikh, T.R., Thomas, D.R., Chen, J.Z., Derosier, D.J., Kitao, A., and Namba, K., Structure of the bacterial flagellar hook and implication for the molecular universal joint mechanism, *Nature* **431**(7095):1062–1068, 2004.
32. Kato, T., Makino, F., Miyata, T., Horváth, P., and Namba, K., Structure of the native supercoiled flagellar hook as a universal joint, *Nature Commun.* **10**:5295, 2019.
33. Shibata, S., Matsunami, H., Aizawa, S.I., and Wolf, M., Torque transmission mechanism of the curved bacterial flagellar hook revealed by cryo-EM, *Nature Struct. Mol. Biol.* **26**:941–945, 2019.
34. Vonderviszt, F. and Namba, K., Structure, function and assembly of flagellar axial proteins | Semantic Scholar, *Madame Curie Bioscience Database*, 2013
35. And up to 1,700 times per second in *Vibrio alginolyticus*: Magariyama *et al.*, ref. 8.
36. Spöring, I., Martinez, V.A., Hotz, C., Schwarz-Linek, J., Grady, K.L., Nava-Sedeño, J.M., Vissers, T., Singer, H.M., Rohde, M., Bourquin, C., Hatzikirou, H., Poon, W., Dufour, Y.S., and Erhardt, M., Hook length of the bacterial flagellum is optimized for maximal stability of the flagellar bundle, *PLOS Biology*, 6 Sep 2018.
37. Nord, A.L., Biquet-Bisquert, A., Abkarian, M., Pigaglio, T., Seduk, F., Magalon, A., and Pedaci, F., Dynamic stiffening of the flagellar hook, *Nature Commun.* **13**:2925, 2022.
38. Green, A.G., Elhabashy, H., Brock, K.P., Maddamsetti, R., Kohlbacher, O., and Marks, D.S., Large-scale discovery of protein interactions at residue resolution using co-evolution calculated from genomic sequences, *Nature Commun.* **12**:1396, 2021.

39. Wang, F., Burrage, A.M., Postel, S., Clark, R.E., Orlova, A., Sundberg, E.J., Kearns, D.B., and Egelman, E.H., A structural model of flagellar filament switching across multiple bacterial species, *Nature Commun.* **8**:960, 2017.
40. Horstmann, J.A., Lunelli, M., Cazzola, H., Heidemann, J., Kühne, C., Steffen, P., Szefs, S., Rossi, C., Lokareddy, R.K., Wang, C., Lemaire, L., Hughes, K.T., Uetrecht, C., Schlüter, H., Grassl, G.A., Stradal, T.E.B, Rossez, Y., Kolbe, M., and Erhardt, M., Methylation of *Salmonella typhimurium* flagella promotes bacterial adhesion and host cell invasion, *Nature Commun.* **11**:2013, 2020.
41. Yamaguchi, T., Toma, S., Terahara, N., Miyata, T., Ashihara, M., Minamino, T., Namba, K., and Kato, T., Structural and functional comparison of salmonella flagellar filaments composed of FljB and FliC, *Biomolecules* **10**(2):246, 2020.
42. Yonekura, K., Maki-Yonekura, S., and Namba, K., Complete atomic model of the bacterial flagellar filament by electron cryomicroscopy, *Nature* **424**:643–650, 2003.
43. Maki-Yonekura, S., Yonekura, K., and Namba, K., Conformational change of flagellin for polymorphic supercoiling of the flagellar filament, *Nat. Struct. Mol. Biol.* **17**:417–422, 2010.
44. Turner, L., Ryu, W.S., and Berg, H.C., Real-time imaging of fluorescent flagellar filaments, *J. Bacteriol.* **182**(10):2793–801, 2000.
45. For a detailed look at the physics behind filament synchronization, see: Tătulea-Codrean, M., and Lauga, E., Elastohydrodynamic synchronization of rotating bacterial flagella, *Phys. Rev. Lett.* **128**:208101, 17 May 2022.
46. Kreutzberger, M., Sobe, R.C., Sauder, A.B., Chatterjee, S., Peña, A., Wang, F., Giron, J.A., Kiessling, V., Costa, T., Conticello, V.P., Frankel, G., Kendall, M.M., Scharf, B.E., and Egelman, E.H., Flagellin outer domain dimerization modulates motility in pathogenic and soil bacteria from viscous environments, *Nature Commun.* **13**:1422, 2022.
47. *The Select Works of Antony Leeuwenhoek*, Tr. Samuel Hoole **2**:214, London, 1816.
48. Jumper, J., Evans, R., Pritzel, A., Green, T., Figurnov, M., Ronneberger, O., Tunyasuvunakool, K., Bates, R., Žídek, A., Potapenko, A., Bridgland, A., Meyer, C., Kohl, S.A. A., Ballard, A.J., Cowie, A., Romera-Paredes, B., Nikolov, S., Jain, R., Adler, J., Back, T., Petersen, S., Reiman, D., Clancy, E., Zielinski, M., Steinegger, M., Pacholska, M., Berghammer, T., Bodenstein, S., Silver, D., Vinyals, O., Senior, A.W., Kavukcuoglu, K., Kohli, P., and Hassabis, D., Highly accurate protein structure prediction with AlphaFold, *Nature* **596**(7873):583–589, 15 Jul 2021.
49. Varadi, M., Anyango, S., Deshpande, M., Nair, S., Natassia, C., Yordanova, G., Yuan, D., Stroe, O., Wood, G., Laydon, A., Žídek, A., Green, T., Tunyasuvunakool, K., Petersen, S., Jumper, J., Clancy, E., Green, R., Vora, A., Lutfi, M., Figurnov, M., Cowie, A., Hobbs, N., Kohli, P., Kleywegt, G., Birney, E., Hassabis, D., and Velankar, S., AlphaFold protein structure database: massively expanding the structural coverage of protein-sequence space with high-accuracy models, *Nucleic Acids Res.* **50**(D1):D439–D444, 17 Nov 2021.
50. Berman, H.M., Westbrook, J., Feng, Z., Gilliland, G., Bhat, T.N., Weissig, H., Shindyalov, I.N., and Bourne, P.E., The protein data bank, *Nucleic Acids Res.* **28**:235-242, 2000 | rcsb.org.
51. Sehnal, D., Bittrich, S., Deshpande, M., Svobodová, R., Berka, K., Bazgier, V., Velankar, S., Burley, S. K., Koča, J., and Rose, A. S., Mol* Viewer: modern web app for 3D visualization and analysis of large biomolecular structures, *Nucleic Acids Res.* **49**:W431–W437, 6 May 2021.
52. Carroll, B.L., Nishikino, T., Guo, W., Zhu, S., Kojima, S., Homma, M., and Liu, J., The flagellar motor of *Vibrio alginolyticus* undergoes major structural remodeling during rotational switching, *eLife* **9**, 7 Sep 2020.
53. Poweleit, N., Ge, P., Nguyen, H.H., Loo, R.R., Gunsalus, R.P., and Zhou, Z.H., CryoEM structure of the *Methanospirillum hungatei* archaellum reveals structural features distinct from the bacterial flagellum and type IV pilus, *Nature Microbiol.* **2**:16222, 5 Dec 2016.
54. Banerjee, A., Tsai, C.L., Chaudhury, P., Tripp, P., Arvai, A.S., Ishida, J.P., Tainer, J.A., and Albers, S.V., FlaF is a β-sandwich protein that anchors the archaellum in the archaeal cell envelope by binding the S-layer protein, *Structure* **23**(5):863–872, 5 May 2015.
55. Gui, M., Farley, H., Anujan, P., Anderson, J.R., Maxwell, D.W., Whitchurch, J.B., Botsch, J.J., Qiu, T., Meleppattu, S., Singh, S.K., Zhang, Q., Thompson, J., Lucas, J.S., Bingle, C.D., Norris, D.P., Roy, S., and Brown, A., De novo identification of mammalian ciliary motility proteins using cryo-EM, *Cell* **184**(23):5791–5806.e19, 11 Nov 2021.
56. Rao, Q., Han, L., Wang, Y., Chai, P., Kuo, Y.W., Yang, R., Hu, F., Yang, Y., Howard, J., and Zhang, K., Structures of outer-arm dynein array on microtubule doublet reveal a motor coordination mechanism, *Nature Structural & Mol. Biol.* **28**(10):799–810, 23 Sep 2021.
57. Gui, M., Ma, M., Sze-Tu, E., Wang, X., Koh, F., Zhong, E.D., Berger, B., Davis, J.H., Dutcher, S.K., Zhang, R., and Brown, A., Structures of radial spokes and associated complexes important for ciliary motility, *Nature Structural & Mol. Biol.* **28**(1):29–37, 14 Dec 2020.
58. Kojima, S., Imada, K., Sakuma, M., Sudo, Y., Kojima, C., Minamino, T., Homma, M., and Namba, K., Stator assembly and activation mechanism of the flagellar motor by the periplasmic region of MotB, *Molecular Microbiol.* **73**:710–718, 2009.

David Thomas *(a pen name) is currently studying biological sciences at university. He was introduced to CMI materials through his parents, both in science fields. David is actively involved in creation apologetics.*